JOURNAL OF GEOPHYSICAL RESEARCH, VOL. 116, D05108, doi:10.1029/2010JD015118, 2011

Double tropopause formation in idealized baroclinic life cycles: The key role of an initial tropopause inversion layer

S. Wang[1] and L. M. Polvani[2]

Received 27 September 2010; revised 29 November 2010; accepted 20 December 2010; published 5 March 2011.

[1] Recent studies have shown that double tropopauses exist in all seasons, and at all longitudes, in the midlatitudes. As of yet, the key mechanism responsible for their formation is not known. In this study, we explore the connection between double tropopauses and midlatitude baroclinic eddies. This is investigated in the context of idealized life cycle experiments. The key finding of this study is that large areas of double tropopauses form spontaneously at the nonlinear stage of the life cycle evolution, provided an extratropical tropopause inversion layer is present in the balanced initial temperature profile. We also show that the areas covered with double tropopauses grow as the strength of the initial tropopause inversion layer is increased. Without such a layer, as in canonical examples of baroclinic life cycles much studied in the literature, no double tropopause formation occurs. In agreement with observations, double tropopauses in our life cycle experiments form predominantly in areas of cyclonic flow at upper levels. However, the air masses that end up between the two tropopauses are found to originate from high latitudes. This appears to differ from a recently published case study, where the air between double tropopauses was shown to originate partly from low latitudes. Such a discrepancy suggests that more than one pathway may exist to advect air masses between the two tropopauses.

Citation: Wang, S., and L. M. Polvani (2011), Double tropopause formation in idealized baroclinic life cycles: The key role of an initial tropopause inversion layer, *J. Geophys. Res.*, *116*, D05108, doi:10.1029/2010JD015118.

1. Introduction

[2] The tropopause marks the boundary between troposphere and the stratosphere. These two regions of the atmosphere possess very distinct dynamical and chemical properties, and the transport of air, moisture and chemical constituents across the tropopause has significant implications for chemistry-climate interactions [*Holton et al.*, 1995; *Stohl et al.*, 2003; *Shepherd*, 2002]. The formation, structure and properties of the tropopause are thus important issues for a complete understanding of dynamical and chemical coupling between the stratosphere and the troposphere.

[3] In simple terms, the tropopause is defined as the height where a discontinuity in the lapse rate is found. However, even early studies [e.g., *Bjerknes and Palmen*, 1937; *Kochanski*, 1955], using upper air soundings, found that vertical profiles of temperature are often characterized by two or more regions of abrupt change in lapse rate, which we now refer to as double or multiple tropopauses (DTs, for short, hereafter). Recent studies using radiosondes, reanalyses and GPS radio occultation profiles [*Schmidt et al.*, 2006; *Randel et al.*, 2007a; *Añel et al.*, 2008; *Castanheira et al.*, 2010] have revealed that DTs are in fact the rule, not the exception.

[4] DTs are ubiquitous, in the midlatitudes (30°–60°), at all longitudes, and in both hemispheres [*Randel et al.*, 2007a]. DTs also have a strong seasonal cycle: their occurrence is maximum during the winter season. Furthermore, DTs are preferentially associated with the presence of cyclonic vorticity at upper levels. And finally, DTs have been found to occur more frequently in the regions of enhanced synoptic activity [*Añel et al.*, 2008] and of Rossby wave breaking [*Pan et al.*, 2009].

[5] These recent findings strongly suggest baroclinic eddies may be closely related to the formation and maintenance of DTs. To date, however, this relationship has not been investigated from a modeling perspective: the goal of this paper is to do so.

[6] As a first step, one might think of revisiting well known baroclinic life cycle experiments (e.g., those in the classic papers of *Simmons and Hoskins* [1980]), and simply diagnosing them to see if regions of DT form spontaneously during the evolution of the flow. We have done so and, perhaps surprisingly, have found *no* DT formation in such cases. More specifically, we have first analyzed model

[1]Department of Applied Physics and Applied Mathematics, Columbia University, New York, New York, USA.

[2]Departments of Applied Physics and Applied Mathematics and Earth and Environmental Sciences, Columbia University, New York, New York, USA.

0148-0227/11/2010JD015118

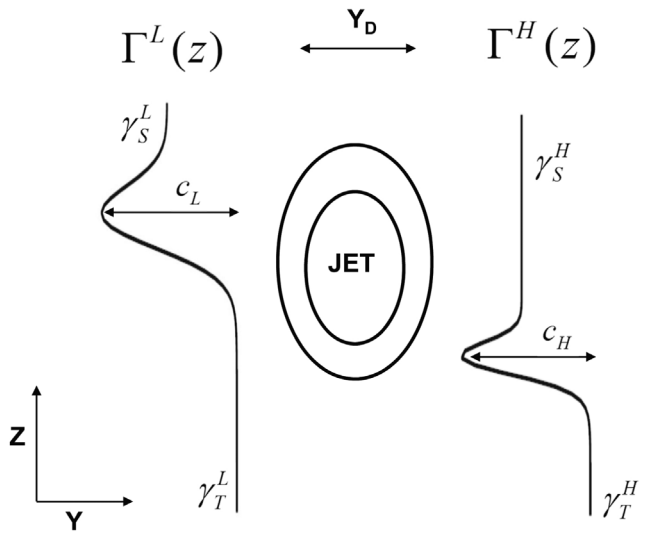

Figure 1. Sketch of the lapse rate pairs $\Gamma^L(z)$ and $\Gamma^H(z)$, at the low and high latitudes, and the resulting baroclinic jet. Y_D is the transition distance between Γ^L and Γ^H and effectively controls the strength of the jet. The parameter c_L controls the value of cold point above the tropopause at low latitudes, and the parameter c_H controls the strength of the extratropical tropopause inversion layer. The four parameters γ_T^L, γ_T^H, γ_S^L, and γ_S^H are the lapse rate constants in the troposphere and stratosphere, at low and high latitudes, respectively.

output from the study of *Polvani and Esler* [2007]: using a global spectral dynamical core, that study closely replicates the original LC1 (dominated by anticyclonic wave breaking) and LC2 (dominated by cyclonic wave breaking) life cycle paradigms proposed by *Thorncroft et al.* [1993]. Second, using WRF (the Weather Research and Forecasting model), we have reproduced the baroclinic life cycle documented by *Rotunno et al.* [1994], who considered an *f*-plane channel flow initialized with piecewise uniform potential vorticity (PV). In both cases no trace of DT formation was found. As these are null results, no figures are shown here. These efforts, however, lead us conclude that the baroclinic instability of a simple jet is not sufficient for DT formation: some other ingredient is needed.

[7] That ingredient is the tropopause inversion layer (TIL). Recently discovered by *Birner et al.* [2002], the TIL is a shallow region of high static stability, typically a couple of kilometers thick, located just above the extratropical tropopause. Similar to DTs, the TIL is a global extratropical phenomenon, covering most longitudes in all seasons [*Birner*, 2006; *Randel et al.*, 2007b; *Bell and Geller*, 2008]. The formation and maintenance of the TIL are not well understood at present, and are the subject of intense current research [*Wirth*, 2003, 2004; *Son and Polvani*, 2007; *Randel et al.*, 2007b; *Kunz et al.*, 2009; *Birner*, 2010; *Randel and Wu*, 2010; *Miyazaki et al.*, 2010].

[8] The key finding of this study is that, if a TIL is present in the initial condition, the evolution of a baroclinic life cycle leads to the formation of large areas of DTs. We demonstrate this by constructing carefully controlled, yet idealized, midlatitude jets with a corresponding balanced temperature profile in which a TIL is present, similar to the one seen in the observations. The strength of the initial TIL can then be controlled by simple parameters, and allows us to demonstrate that the area of DTs formed during the nonlinear stages of the baroclinic life cycle grows as the strength of the initial TIL is increased.

[9] The paper is laid out as follows. In section 2 we present, in detail, how balanced initial winds and temperatures are constructed, and we briefly describe the numerical scheme used to obtain nonlinear solutions and the algorithm used to identify DTs. In section 3 we show how DTs emerge spontaneously during baroclinic life cycles, and how they depend on the strength of the initial TIL. We use idealized tracers to determine the source of air that is eventually found between the two tropopauses. And we also consider how the area of DTs generated during the life cycle evolution depends on the type of life cycle. A brief discussion closes the paper in section 4.

2. Methods

2.1. Initial Conditions

[10] We first describe the procedure used for constructing baroclinically unstable initial winds and temperature, in thermal wind balance, with a TIL of a desired strength. Unlike *Rotunno et al.* [1994], who start by specifying PV and then perform an inversion, or *Polvani and Esler* [2007], who start by specifying winds and then obtain temperature by balancing, we here start by specifying temperature (actually, lapse rate), since we need to control the location and amplitude of the TIL.

[11] The key elements of our initialization are sketched in Figure 1. The starting point is a pair of lapse rate profiles, $\Gamma^L(z)$ and $\Gamma^H(z)$, at low and high latitudes with respect to the jet, respectively. (The lapse rate in this study is defined as the vertical derivative of temperature, $\Gamma = -\frac{dT}{dz}$, where $z = -H \ln(p_0/p)$ is the pseudo-height, the scale height H = 7.5 km, p is pressure, and p_0 = 1000 hPa. The use of pseudo-height here (instead of the geometric height z), greatly simplifies the initialization procedure.) Each of these profiles requires several parameters: the lapse rate in the troposphere and the stratosphere, the height of the tropopause, and the thickness and strength of the TIL. These two profiles are blended together with a hyperbolic tangent in y (the latitude), over a distance Y_D, to form the single lapse rate $\Gamma(z, y)$ that applies over the entire domain. From $\Gamma(z, y)$ the temperature at any point is easily obtained by integrating down from the top of the model (we take the model atmosphere to be isothermal above a certain height). With the temperature in hand, the balanced winds are then computed by integrating the thermal wind equation from the surface upward, assuming zero wind at the surface. To ensure reproducibility of our results, complete details of this initialization procedure (including all analytical formulas and all the values of parameters used) are given in Appendix A1.

[12] For the sake of clarity, we will mostly be focussing on a set of four initial conditions, illustrated in Figure 2. These differ, primarily, in the strength of the TIL, shown by the shaded regions on the poleward of the jet: case TIL_None has no TIL, and the other cases have a weak, medium and strong TIL. These initial conditions are obtained by using four different values of the parameter c_H (see Figure 1).

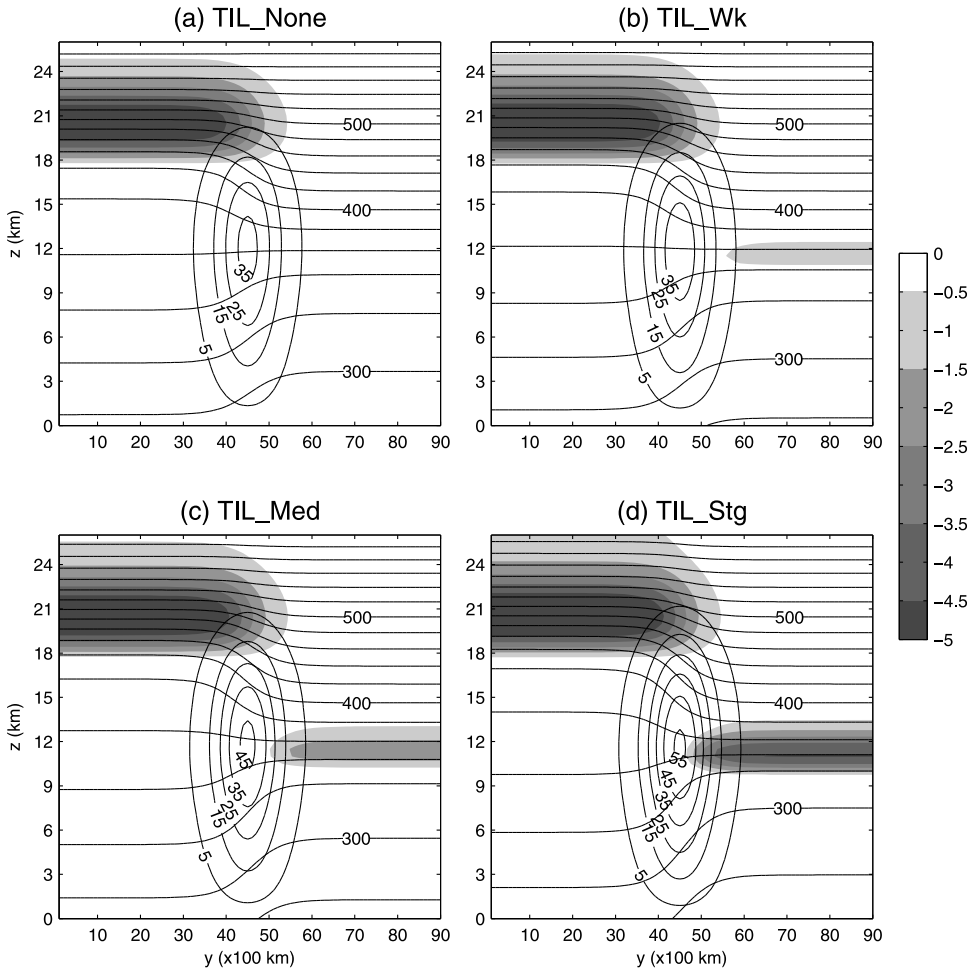

Figure 2. Contours show zonal winds (contour interval 10 m s^{-1}) and potential temperature (contour interval 20 K) for four initial conditions with progressively stronger TIL. Shaded areas show the lapse rate $-dT/dz$, in K km^{-1}. The corresponding parameter values are given in Tables 1 and A1.

We note that in order to have a closed jet at the tropopause, it is necessary to change the value of the parameter γ_S^L (again, see Figure 1) together with the c_H. The values of these parameters for each of the cases in Figure 2 are given in Table 1. Note that the jet strength also varies among these different cases: its impact will be discussed later.

[13] For clarity, we show in Figure 3 the lapse rates, on both sides of the jet, corresponding to each of the four cases. The lapse rate $\Gamma^L(z)$ on the equatorward side of the jet, shown by the dashed lines, is associated with the tropical tropopause, is nearly identical in all cases. In contrast, the lapse rate $\Gamma^H(z)$ on the poleward side of the jet, associated with the TIL, shows an increasing amplitude of the inversion, from TIL_Wk to TIL_Med to TIL_Stg. Note that the thickness of TIL is comparable on both sides of jet in Figure 3, whereas observations show that it is thicker in high latitudes [*Bell and Geller*, 2008]. This slightly unrealistic feature is not crucial for the results presented in this work.

2.2. Model Numerics

[14] Given the above winds and temperatures, we use the nonhydrostatic Weather Research and Forecasting (WRF) model [*Skamarock et al.*, 2008], version 3.0, to carry out the baroclinic life cycle experiments presented in this study. The WRF model is set up to run in an idealized configuration, i.e., only dry dynamics on an *f*-plane channel, with a constant Coriolis parameter $f = 1 \times 10^{-4}$ s^{-1}, is included. Periodic boundary conditions are adopted in the *x* direction; rigid wall conditions in *y*. The vertical coordinate is exponentially stretched such that vertical spacing is nearly constant in *z*.

[15] For our standard integrations, the computational domain is 5000 km × 9000 km × 28 km in the *x*, *y* and

Table 1. Key Parameters Used to Produce the Four Initial Conditions Illustrated in Figures 2 and 3[a]

	c_H (K km^{-1})	γ_S^L (K km^{-1})
TIL_None	0	0
TIL_Wk	0.25	−0.139
TIL_Med	0.5	−0.278
TIL_Stg	1.0	−0.555

[a]The TIL amplitude at high latitudes is given by c_H, and γ_S^L is the lapse rate in the stratosphere at low latitudes. In all cases, $Y_D = 750$ km. All other parameters are given in Table A1.

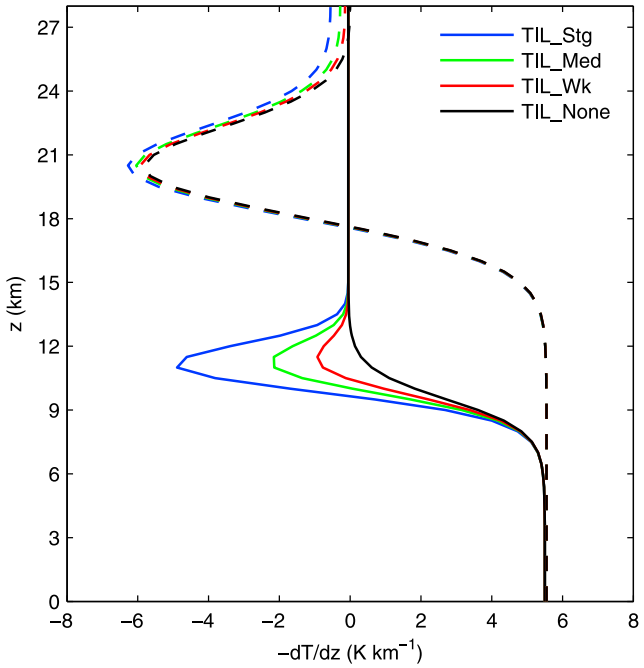

Figure 3. Solid lines are the lapse rate $\Gamma^H(z)$ of the poleward side of the jet, associated with the extratropical TIL. Dashed lines are the lapse rate $\Gamma^L(z)$ of the equatorward side of the jet, associated with the cold-point tropical tropopause. Colors refer to the different initial cases shown in Figure 2, as indicated in the legend.

z directions, and we choose a grid spacing of 100 km in x and y, and 450 m (approximately) in z. This results in a grid of 51 × 91 × 61 points. For convenience, the horizontal y dimension is referred as the latitude, in analogy to similar studies in the spherical geometry.

[16] The advection scheme for the dynamical variables is 5th order for the horizontal and 3rd order for the vertical direction. The advection of the passive tracers, discussed in section 3.3, is done with a standard positive definite advection scheme [*Skamarock et al.*, 2008]. All these schemes are inherently diffusive, so there is no need to specify any explicit diffusion.

2.3. Tropopause Detection Algorithm

[17] The location of thermal tropopauses are defined by the *World Meteorological Organization* [1957] as follows. The first tropopause is the lowest altitude at which the lapse rate decreases to 2 K km^{-1} provided the average lapse rate between this level and all higher levels within 2 km does not exceed 2 K km^{-1}. If above the first tropopause the average lapse rate between any level and all higher levels within 1 km exceeds 3 K km^{-1}, then a second tropopause is defined by the same criterion; this second tropopause may be either within or above the 1 km layer.

[18] We adopt the above WMO definition but, following *Randel et al.* [2007a], we modify the 3 K km^{-1} criterion to 2 K km^{-1} when identifying the second tropopause. We also note that, in WRF, the height and temperature on each model level are available without any interpolation, using the standard hydrostatic pressure vertical coordinates. The tropopause height thus is obtained by linearly interpolating height with respect to the lapse rates to obtain the altitude at which lapse rate equals to 2 K km^{-1}.

3. Results

3.1. Baroclinic Life Cycles

[19] Although different in TIL strength, all the profiles shown in Figure 2 are baroclinically unstable owing to the strong vertical wind shear near the surface. We employ small, idealized initial temperature perturbations, as detailed in Appendix A2, to break the initial zonal symmetry and allow the most unstable normal mode to emerge, and then follow the instability as it develops to finite amplitude.

[20] The resulting life cycles are illustrated in Figure 4, where we plot PV on the θ = 335 K isentropic surface. Areas with PV above the 2 PVU value are simply shaded in gray, to differentiate stratospheric from tropospheric air. Figures 4a–4d show the evolution of the four conditions presented in Figure 2. The rows illustrate different stages: linear growth at the top, maximum eddy kinetic energy (EKE) in the middle row, and barotropic decay at the bottom.

[21] In terms of gross features, these life cycles are quite similar. The EKE peaks around 7–10 days, and the life cycle completes in about 20 days. In all four cases, as illustrated in Figure 4, large cyclonic regions of stratospheric air are pinched off in the middleworld, with corresponding cut-off cyclones near the surface (not shown). These features are characteristic of LC2 type life cycles, as described by *Thorncroft et al.* [1993].

[22] We note that no additional shear is needed to produce LC2 life cycles on the *f*-plane in Cartesian geometry, in agreement with many previous studies [e.g., *Snyder et al.*, 1991; *Rotunno et al.*, 1994; *Bush and Peltier*, 1994; *Zhang*, 2004]. This is in contrast to what is found in spherical geometry, where additional meridional shear is needed to produce LC2 life cycles [e.g., *Hartmann*, 2000]. This interesting difference was discussed by *Whitaker and Snyder* [1993].

3.2. Double Tropopause Formation

[23] The key finding of this paper is illustrated by the red areas shown in Figure 4: these mark the locations where double tropopauses form, as determined using the algorithm described in section 2.3. As seen in Figure 4, substantial areas of DTs spontaneously emerge during the life cycle evolution, and are found to be progressively larger as the initial TIL is stronger.

[24] To quantify the DT formation process, we compute the quantity $\mathcal{A}_{DT}$, the fractional area of the computational domain, in the midlatitudes (i.e., between y = 3000 and 6500 km), covered by DTs. A value of 1 indicates the presence of DTs everywhere in the midlatitudes.

[25] The evolution of this quantity, for all four life cycles, is shown in Figure 5a. Although the different life cycles develop at slightly different rates owing to the different initial baroclinicity (cf. the initial jet strength), in all cases $\mathcal{A}_{DT}$ starts to grow rapidly a few days after the EKE peaks (as indicated by the stars in Figure 5a), and reaches its maximum 6 to 7 days later. This suggests that chaotic advection in the nonlinear stages of the wave breaking is important for DT development. For the four life cycles in Figure 4, the change in $\mathcal{A}_{DT}$ is reported in the top row of

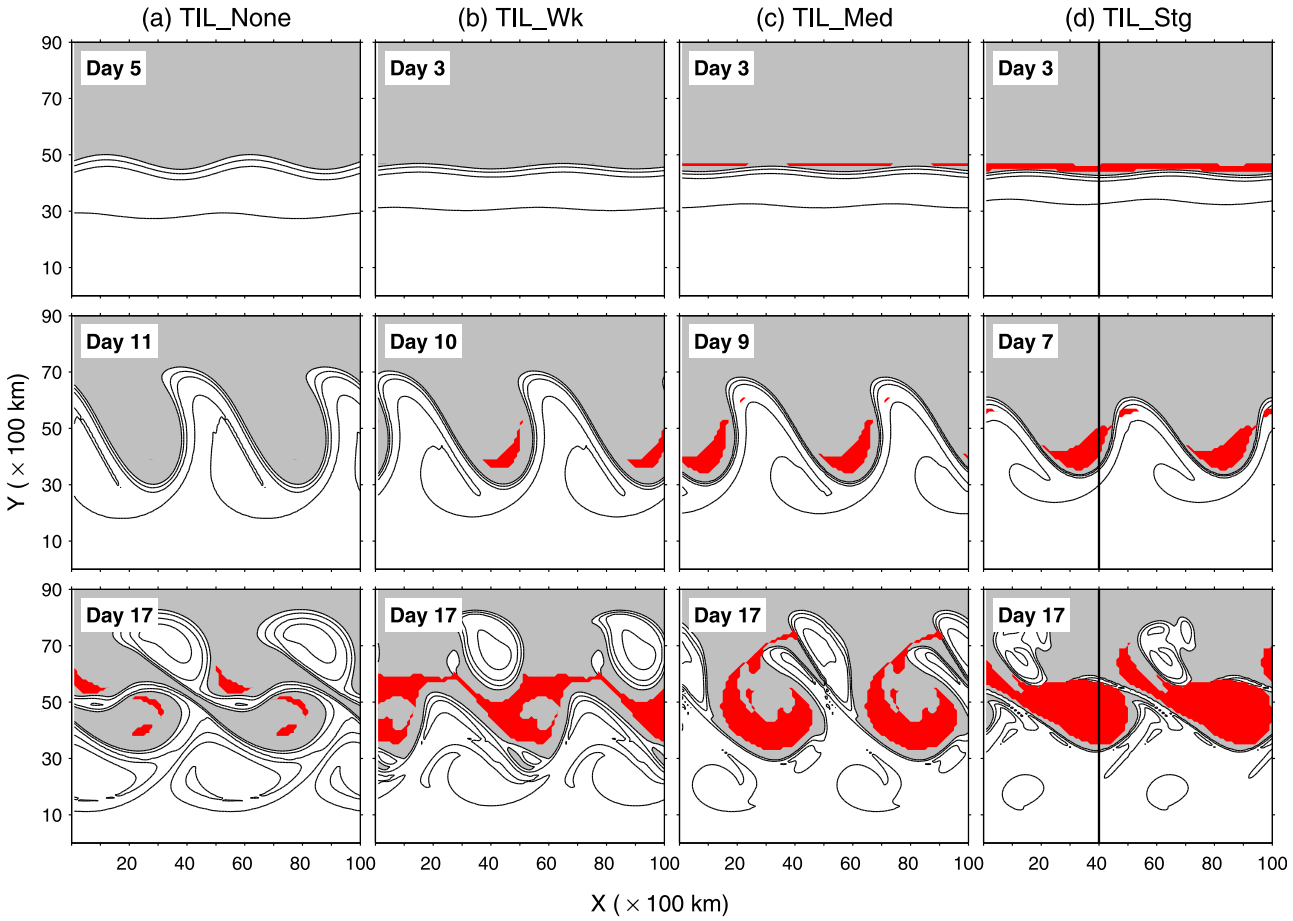

Figure 4. PV on the 335 K surface for the four initial conditions in Figure 2, at selected times: (top) linear growth, (middle) maximum eddy kinetic energy, and (bottom) barotropic decay. The contour interval is 0.5 PVU, and values above 2 PVU are shaded in gray. For clarity, two wavelengths are shown. The red areas mark the regions where double tropopauses are present.

Table 2, together with the value of the jet maximum in the corresponding initial condition (see below in this section).

[26] Next, we demonstrate that the DTs formed during our life cycle evolution are highly correlated with the regions of cyclonic vorticity, as reported in the observational analyses of *Randel et al.* [2007a]. This is shown in Figure 5b, where we have partitioned $\mathcal{A}_{DT}$ according to the sign of vorticity at 200 hPa. It is abundantly clear that DTs are almost totally associated with regions of cyclonic vorticity at upper levels in our numerical integrations. This finding is not unexpected from a dynamical point of view, given that the flows in our integrations are approximately geostrophically and hydrostatically balanced, as pointed out by *Randel et al.* [2007a]. Nonetheless, the fact that DTs form spontaneously during the life cycle evolution is not immediately obvious, and offers one possible explanation for the observed asymmetry between cyclonic and anticyclonic regimes.

[27] Given the sensitive nature of baroclinic development, it is important to clarify the degree to which the above results are sensitive to the numerical resolution at which the integrations are performed. To numerically validate our results we have computed several solutions, with an identical TIL_Stg initial condition, but with doubled and halved grid sizes, both horizontally (Δx) and vertically (Δz). The results are shown in Figure 6, and confirm the robustness of the key finding of our study: the spontaneous formation of DTs during the life cycle evolution. When the resolution is coarsened (blue curves) quantitative differences become noticeable, but the qualitative result is still there. When the resolution is refined (red curves) the results are very similar to the ones in the reference solution (black curve).

[28] The acute reader might have noticed that, in addition to the strength of the TIL, the initial conditions in Figure 2 differ in another potentially important respect: the strength of the jet, which increases progressively as the TIL strengthens. This is due to the fact that it is difficult to

Table 2. The Maximum Zonal Wind $U_{\max}$ of the Initial Jet (in m s^{-1}) and the Net Change $\delta\mathcal{A}_{DT}$ in the Fractional Area Covered by DTs (From Day 0 to Its Maximum Value), as a Function of the Initial TIL and the Parameter Y_D[a]

Y_D/Case	TIL_None		TIL_Wk		TIL_Med		TIL_Stg	
	$U_{\max}$	$\delta\mathcal{A}_{DT}$	$U_{\max}$	$\delta\mathcal{A}_{DT}$	$U_{\max}$	$\delta\mathcal{A}_{DT}$	$U_{\max}$	$\delta\mathcal{A}_{DT}$
750 km	38.2	0.1	42.8	0.27	47.5	0.33	56.9	0.37
850 km	33.8	0.08	37.8	0.28	42.0	0.36	50.3	0.40
950 km	30.3	0.01	33.9	0.25	37.6	0.33	44.1	0.48

[a]See text.

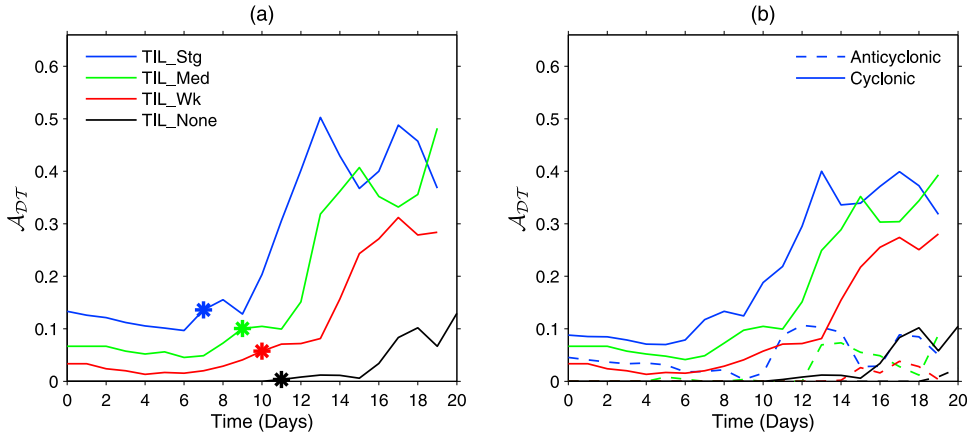

Figure 5. (a) Time series of the $\mathcal{A}_{dt}$, the fractional area of DTs in the midlatitudes, for the four baroclinic life cycles in Figure 4. The stars indicate the times of maximum eddy kinetic energy. (b) Time series of $\mathcal{A}_{DT}$ within regions of anticyclonic shear (dashed) and cyclonic shear (solid), defined using relative vorticity at 200 hPa. In all cases, Y_D = 750 km.

control all aspects of the initial flow with a relatively small number of parameters. Nonetheless, one might wonder whether our interpretation is possibly erroneous, and the formation of DTs is due to a strong jet instead of a strong TIL. To address this issue, we have computed two more sets of four life cycles each: the new sets are identical to the original one in all respects except for the parameter Y_D, which is varied from the original value of 750 km, to 850 km and 950 km. Varying this parameter allows us to control the speed of the initial jet (as can be seen from Figure 1).

[29] The results are illustrated in Figure 7. In all cases, a stronger TIL leads to larger areas of DTs. The key point, however, can be gathered from Table 2, where results for the new sets are tabulated in the second and third rows. Comparing results by reading downward along any column, one can see that the initial wind maximum decreases in all cases, while the TIL changes little and not always monotonically. Alternatively, consider the cases on the main diagonal (starting from the top left) in Table 2: in all three cases the initial wind maximum is close to 38 m s^{-1} (38.2, 37.9 and 37.6) while the increase in $\mathcal{A}_{DT}$ is very different depending on the initial TIL (it varies from 0.1 to 0.28 to 0.33), confirming our conclusion that the initial TIL is the principal controlling factor, given sufficient jet strength.

3.3. Air Mass Mixing

[30] In this section we wish to determine the latitudinal origin of the air masses that end up in the region between the two tropopauses at the end of each baroclinic life cycle. To answer this question, we initialize a passive tracer with the value of the corresponding y coordinate at each grid point, and simply advect it during the numerical integration. The results are given in Figure 8, for the TIL_Stg case, where we show a cross section of the flow at longitude X = 4000 km (cf. the black vertical line in Figure 4d), at several stages of the life cycle evolution. The other TIL cases are qualitatively similar but with weaker DTs, as already shown.

[31] Consider first the DT formation process. The location of the tropopauses at this particular longitude, as determined with the algorithm described in section 2.3, are shown by the black dots in Figure 8. Note that the meridional width of the region with DTs increases dramatically in meridional extent: from 200 km at day 3, to 1500 km at day 7, and to more than 2000 km at at day 17. While this number may appear large, is it quite similar to the meridional extents that have been reported in observations [see, e.g., *Pan et al.*, 2009, Figures 1 and 3].

[32] Next, the evolution of air masses can be seen from the red and blue colors in Figure 8, which track air masses initially located at high and low latitudes, respectively. At day 3 only small perturbations appear but, by day 7 (middle

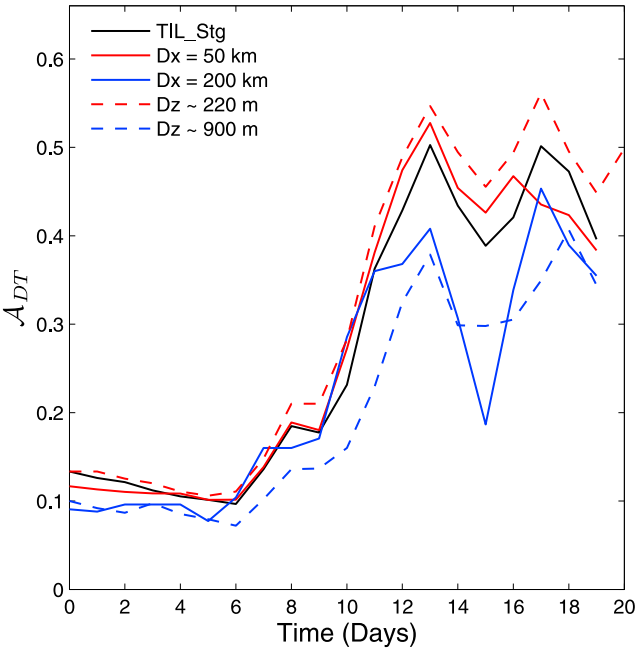

Figure 6. As in Figure 5a, but for experiments at different horizontal and vertical resolutions. Black curve is the reference solution with Δx = 100 km and $\Delta z \sim$ 450 m. Color curves show different resolution, as indicated in the legend. All integrations are for the TIL_Stg initial condition shown in Figure 2d.

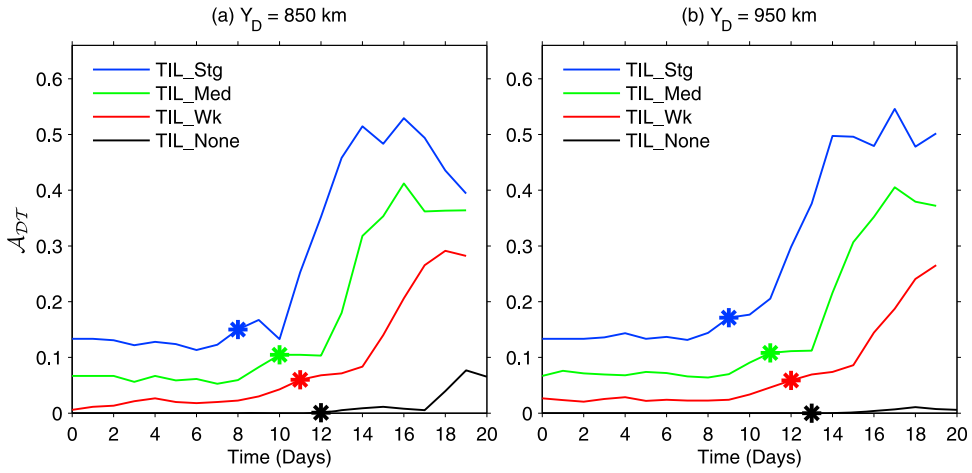

Figure 7. As in Figure 5a, but for numerical experiments with Y_D = (a) 850 km and (b) 950 km.

panel), significant meridional transport of air masses is found along this cross section. Specifically, the region between the two tropopause is predominantly composed of air that is being advected there from high latitudes, whereas low-latitude air, advected poleward, is found both below the lower tropopause and above the upper tropopause. These features persist later in the life cycle, as can be seen in the bottom panel at day 17. Finally, we note that these broad features are not peculiar to this particular example, but are representative of all the life cycle integrations discussed in this paper.

[33] It is interesting to relate Figure 8 with the two intrusion events reported by *Pan et al.* [2009], where DTs were observed using satellite remote sensing data from High-Resolution Dynamics Limb Sounder (HIRDLS) instrument on the Aura satellite, in combination with ozonesonde data and high-resolution meteorological analyses. In those events the air sandwiched between the two tropopauses was determined, using Lagrangian trajectories techniques, to have partly originated at low latitudes. In our idealized cases we find, on the contrary, that the air found in the DT region originated almost uniquely at high latitudes, and we have found this to be the case in every one of many integrations we have performed.

3.4. Anticyclonic (LC1) Life Cycles

[34] Up to this point, the entire discussion has been limited to the cyclonic type of baroclinic life cycle (referred to as LC2 in the literature). However, as demonstrated by *Polvani and Esler* [2007], the type of baroclinic life cycles (LC1 versus LC2) had a very significant impact on tracer transport across the tropopause. This raises the question of how LC1 and LC2 may differ in terms of DT formation. In this section we discuss LC1 life cycles, and document how they differ from LC2 ones.

[35] To set up an LC1, we simply add a barotropic, anticyclonic shear to the initial conditions for the TIL_Stg case. This additional shear, of amplitude u_s, is chosen to be similar to the one used by *Hartmann* [2000]; all details are to be found in Appendix A3. For u_s = 10 m s^{-1} the initial condition is shown in Figure 9 and can be directly contrasted with the one in Figure 2d.

[36] The evolution of the LC1 initial condition is illustrated in Figure 10, which shows PV on θ = 335 K and the region of double tropopauses (in red) at three stages during the life cycles, chosen as in Figure 4d, to which it should be compared. Notice the formation of anticyclonic PV tongues, typical of LC1 life cycles. More importantly, note how the areas of DTs are comparatively small in the end, as the flow is not dominated by the large cyclonic structures typical of LC2 life cycles.

[37] We quantify DT formation in LC1 life cycles in Figure 11, where one can compare the area of DTs with the LC2 case (dashed black curve). The blue curve shows the area of DTs for the life cycle shown in Figure 10. Note how, in the LC1 case, the area of DTs actually decreases with time, and ends up being very small compared with the LC2 case. To test the robustness of this result we have computed two additional LC1 life cycles, with stronger and weaker barotropic shears (u_s = 12.5 and 7.5 m s^{-1}); they are shown by the green and red curves, respectively. The bottom line is clear: DT formation in LC1 is very weak compared with LC2, as one might have guessed from the relationship between DT and upper level vorticity.

4. Discussion

[38] Recent observational studies of double tropopauses [*Schmidt et al.*, 2006; *Randel et al.*, 2007a; *Añel et al.*, 2008] have shown that they are ubiquitous, occur in all seasons, and are found primarily in the midlatitudes. Since the origin of DTs is as yet unknown, and since the midlatitudes is where baroclinic eddies are found, this study has investigated the connection between DT formation and synoptic-scale eddies, to see if these might play some role in the formation of DTs.

[39] The key finding of this study is that DTs form spontaneously during life cycle evolution, provided an initial TIL is present. Canonical examples of baroclinic life cycles [e.g., *Thorncroft et al.*, 1993; *Rotunno et al.*, 1994] yield no DTs. If however, a TIL is present in the initial

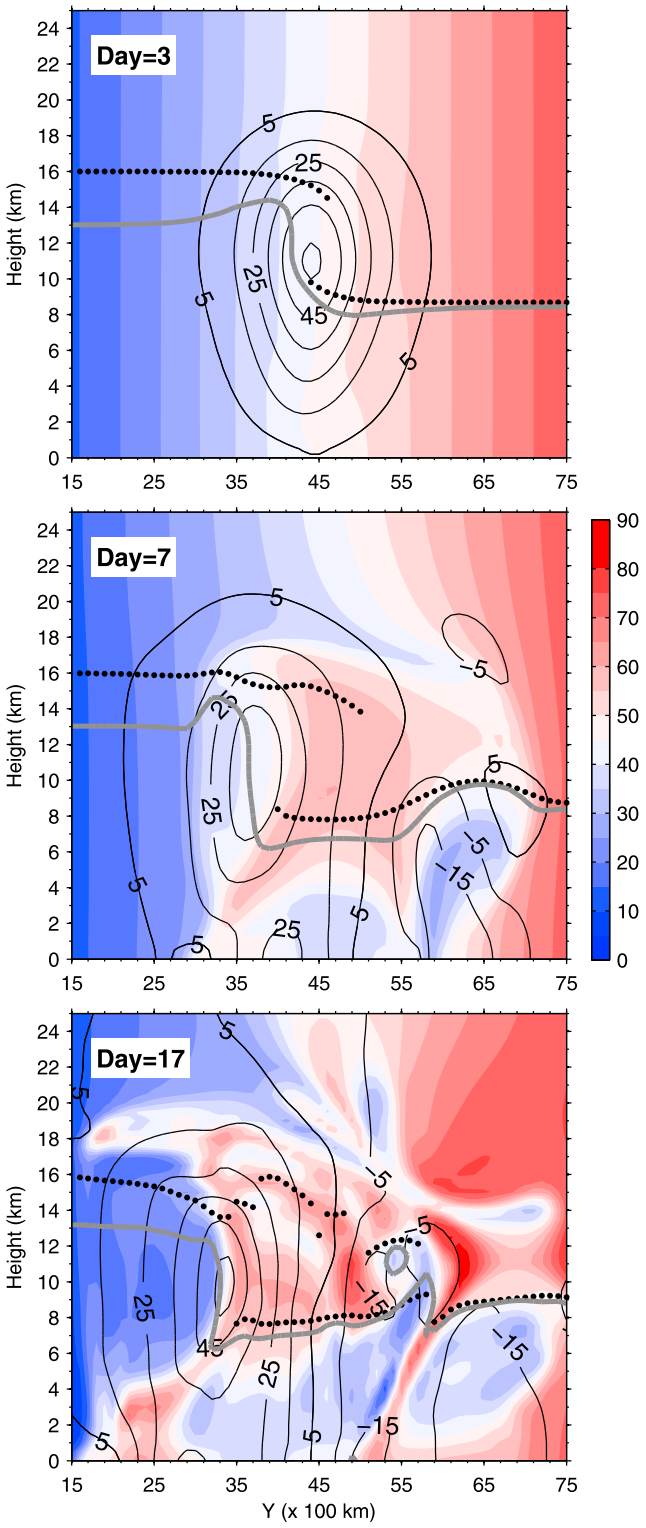

Figure 8. Tropopause (dotted), passive tracer initialized with the value of the corresponding y coordinate (shading), PV (2 PVU, gray), and wind speed (every 5 m s^{-1} from 20 m s^{-1}) along the cross sections in TIL_Stg at X = 4000 km at day 3, 7, and 17, indicated by the solid lines in Figure 4d.

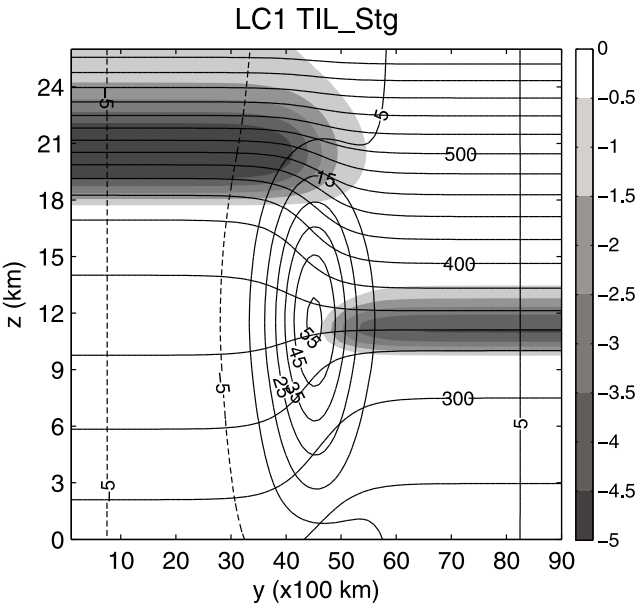

Figure 9. As in Figure 2d, but with an additional barotropic and anticyclonic wind shear, with an amplitude of 10 m s^{-1} (see section A3 for details), to generate an LC1 life cycle.

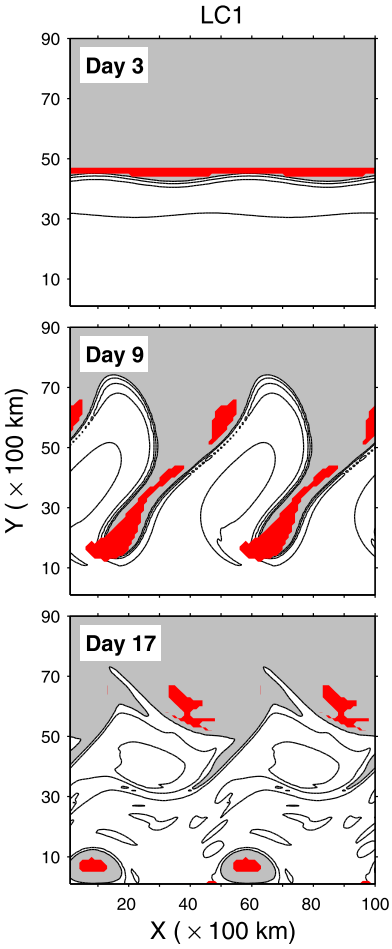

Figure 10. As in Figure 4d, but for the LC1 initial conditions in Figure 9.

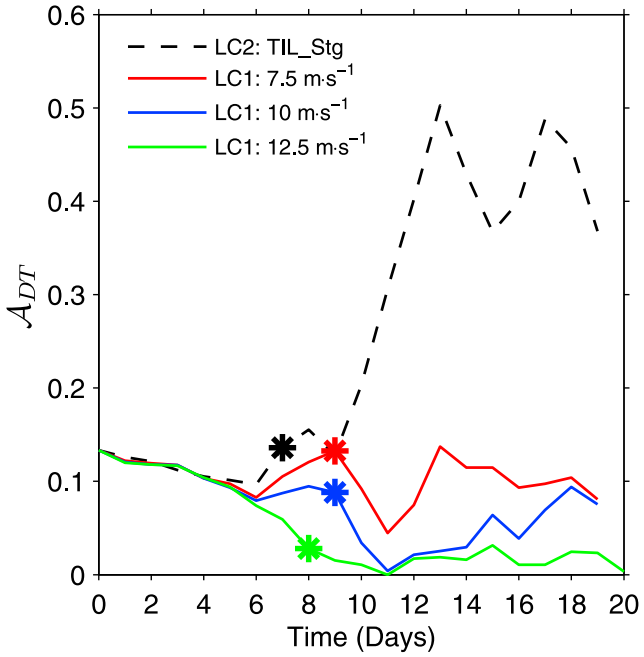

Figure 11. As in Figure 5a, but for three different LC1 life cycles, initialized with a barotropic shear u_s = 7.5 m s^{-1} (red), 10 m s^{-1} (blue) and 12.5 m s^{-1} (green). The black, dashed line show the corresponding LC2 case, for direct comparison. All these life cycles were initialized with a TIL_Stg set of parameters.

conditions, large areas of DT emerge at the nonlinear stages of the life cycle evolution, and these areas grow with the strength of the initial TIL.

[40] Furthermore, in agreement with observations, our model integrations show that DTs form predominantly in areas of cyclonic flow at upper levels, as found in the observations [*Randel et al.*, 2007a]. For the same reason, the formation of DT during baroclinic life cycles is found to depend greatly on the life cycle type, with LC2 life cycles being the overwhelming source of DTs.

[41] We have also shown that, in the idealized life cycles we have considered, the air masses that are found between the two tropopauses at the end of the life cycle originate mostly from high latitudes. This appears to differ from recently published case studies by *Pan et al.* [2009], where the air between the DTs partly originated from the low latitudes. The reason for this difference is unclear at present, and further work is needed to understand it. However, our idealized study suggests that more than one pathway may exist to advect air masses between the two tropopauses.

[42] Finally, we comment on the climatology of the TIL and the DTs, and what can be learned from their differences. While both DTs and TILs are found in the extratropics and in all seasons, their climatologies are different in two key aspects. First, the seasonal cycle of TIL and DTs are nearly opposite: DTs are most abundant in winter season [*Randel et al.*, 2007b, 2007a], while TIL is strongest in the summer season [*Birner*, 2006]. Second, their correlation with the upper tropospheric vorticity is also opposite: DTs are highly correlated with cyclonic circulation systems, while the TIL is much stronger in anticyclones.

[43] These opposite behaviors between DTs and TIL might appear difficult to reconcile with our results, since we have shown that stronger TIL leads to more DTs in idealized life cycles. However, we argue that mixing by baroclinic eddies can still be a key player in DT formation if one takes into account the seasonality of synoptic-scale eddies themselves. Because these are much more pronounced during the winter season in the region of storm tracks, it is thus reasonable to expect more DT formation in winter. This may explain why the observed DTs are more frequent in winter, while the seasonal cycle of TIL may be related to enhanced water vapor near the tropopause through radiative influence [e.g., *Randel et al.*, 2007b; *Randel and Wu*, 2010; *Miyazaki et al.*, 2010].

[44] Our study may be thought of, in the end, as a simple first step toward understanding the formation and maintenance of double tropopauses. Many possibly important physical processes were not considered here, e.g., large-scale topography, moist processes, etc. These factors may also play important roles. Where, when and how much will be the subject of future research.

Appendix A: Initialization of Baroclinic Life Cycles

[45] Since the procedure for initializing the baroclinic life cycles discussed in this study is relatively cumbersome, we have relegated to this appendix all details necessary to fully reproduce our model integrations.

A1. Basic State, Temperature, and Zonal Winds

[46] The temperature field $T(y, z)$ is constructed by choosing the lapse rate $\Gamma(z) = -\frac{dT}{dz}$, where $z = -H \ln(p_0/p)$ is the pressure height, p is pressure, H = 7.5 km is the scale height, and p_0 = 1000 hPa. We start by first defining the low- and high-latitude lapse rate profiles $\Gamma^L(z)$ and $\Gamma^H(z)$, as follows:

$$\Gamma^L(z) = \left\{\gamma_T^L + \left(\gamma_S^L - \gamma_T^L\right)\cdot\left[\frac{1}{2} + \frac{1}{2}\tanh\left(\frac{z - z_T^L}{z_D^L}\right)\right]\right\} + \left\{c_L \cdot \exp\left[-\left(\frac{z - z_{TIL}^L}{z_{DTIL}^L}\right)^2\right]\right\} \quad \text{(A1)}$$

and

$$\Gamma^H(z) = \left\{\gamma_T^H + \left(\gamma_S^H - \gamma_T^H\right)\cdot\left[\frac{1}{2} + \frac{1}{2}\tanh\left(\frac{z - z_T^H}{z_D^H}\right)\right]\right\} + \left\{c_H \cdot \exp\left[-\left(\frac{z - z_{TIL}^H}{z_{DTIL}^H}\right)^2\right]\right\} \quad \text{(A2)}$$

[47] The key parameter of interest for this paper is c_H, which controls the *amplitude* of tropopause inversion layer, as illustrated in Figure 1. The value of c_L controls the cold point temperature at low latitudes. The parameters γ_S^L and γ_T^L are constant lapse rates at low latitudes, in the stratosphere and troposphere, respectively; similarly for γ_S^H and γ_T^H at high latitudes. At low latitudes, the parameters z_T^L and z_D^L control the tropopause height and extent, and z_T^H and z_D^H do the same at high latitudes. The location and thickness of the TIL is controlled by the parameters z_{TIL}^L and z_{DTIL}^L,

Table A1. Parameters Used for Constructing the Initial Conditions

c_H	See Table 1
c_L	1.25 K km^{-1}
γ_T^H	5.5 K km^{-1}
γ_T^L	5.55 K km^{-1}
γ_S^H	−0.055 K km^{-1}
γ_S^L	see Table 1
z_T^H	10 km
z_T^L	19 km
z_D^H	1.5 km
z_D^L	2.5 km
z_{TIL}^H	11.5 km
z_{TIL}^L	21.5 km
z_{DTIL}^H	1.5 km
z_{DTIL}^L	1.5 km
Y_0	4500 km
Y_D	750 km
z_{top}	28 km
T_{top}	220 K
F	10^{-4} s^{-1}
R	287 J kg^{-1} K^{-1}
H	7.5 km

respectively, at low latitudes, with corresponding parameters z_{TIL}^H and z_{DTIL}^H at high latitudes.

[48] Next, the expression for $\Gamma^H(z)$ and $\Gamma^L(z)$ are combined to construct the lapse rate $\Gamma(y, z)$ as follows:

$$\Gamma(y,z) = \Gamma^L(z) + \left(\Gamma^H(z) - \Gamma^L(z)\right) \cdot \left[\frac{1}{2} + \frac{1}{2}\tanh\left(\frac{y - Y_0}{Y_D}\right)\right] \tag{A3}$$

where Y_0 is the center latitude of the jet, and Y_D is the width of the jet (and also controls the strength of the jet).

[49] Finally, the temperature $T(y, z)$ is obtained by integrating $\Gamma(y, z)$ from a high altitude, where the model atmosphere is a chosen to be isothermal. Setting $T = T_{top}$ at $z = z_{top}$ yields

$$T(y,z) = T_{top} + \int_{z_{top}}^{z} \Gamma(y,s)ds \tag{A4}$$

The values of all parameters used in this study are given in Table A1.

[50] Once the temperature is known, the zonal wind $U(y, z)$ is easily obtained from the thermal wind balance

$$f\frac{\partial u}{\partial z} = -\frac{R}{H}\frac{\partial T}{\partial y} \tag{A5}$$

which is integrated assuming $U(y, 0) = 0$ to yield

$$U(y,z) = -\frac{R}{fH}\int_0^z \frac{\partial T(y,t)}{\partial y}dt \tag{A6}$$

Since the lapse rate is analytically specified, the integrand can be evaluated exactly, so that

$$U(y,z) = \frac{R}{2fHY_D}\left[1 - \tanh^2\left(\frac{y - Y_0}{Y_D}\right)\right]\int_0^z dt \cdot \int_{ztop}^{t} ds\left[\Gamma^H(s) - \Gamma^L(s)\right] \tag{A7}$$

The numerical integrations in (A4) and (A7) are carried out using a simple trapezoid rule. To further ensure that the initial wind and temperature is balanced in terms of the model's numerical scheme, an initially zonal, 20 day run is performed for each experiment. Time averaged wind and temperature from the output of that run are then used as the fully balanced initial conditions.

A2. Initial Perturbation

[51] An iterative procedure, as given by *Plougonven and Snyder* [2007], is adopted to extract the fastest growing baroclinic modes. An initial small perturbation centered in the middle of the domain, following equation 10 of *Polvani and Esler* [2007], with the amplitude of 0.5 K is added to potential temperature (for simplicity, since this is the prognostic variable in WRF). At day 4, the nonzonal component of the solution is extracted and rescaled, so as to having maximum amplitude of 0.5 K for the potential temperature field. This rescaling is iterated four times, after which the fastest growing mode is obtained.

A3. Anticyclonic Life Cycles

[52] To construct anticyclonic life cycles (i.e., of type LC1), we add to the expression in equation (A7) a zonal barotropic wind component $U_s(y)$ with anticyclonic meridional shear and barotropic vertical structure. Taking our inspiration from *Hartmann* [2000], we use

$$U_s(y) = u_s\left\{-\exp\left(-\left(\frac{y - 2000\text{ km}}{1500\text{ km}}\right)^2\right) + \exp\left(-\left(\frac{y - 7000\text{ km}}{1500\text{ km}}\right)^2\right)\right\} \tag{A8}$$

where u_s determines the strength of the barotropic shear.

[53] **Acknowledgments.** We thank Bill Randel, Chris Snyder, Fuqing Zhang, Laura Pan, and Kenneth Bowman for useful discussions. We are grateful to Marvin Geller, Volkmar Wirth, and an anonymous reviewer for their valuable comments on the manuscript. This work is funded, in part, by a grant from the U.S. National Science Foundation to Columbia University.

References

Añel, J. A., J. C. Antuña, L. de la Torre, J. M. Castanheira, and L. Gimeno (2008), Climatological features of global multiple tropopause events, *J. Geophys. Res.*, *113*, D00B08, doi:10.1029/2007JD009697.

Bell, S. W., and M. A. Geller (2008), Tropopause inversion layer: Seasonal and latitudinal variations and representation in standard radiosonde data and global models, *J. Geophys. Res.*, *113*, D05109, doi:10.1029/2007JD009022.

Birner, T. (2006), Fine-scale structure of the extratropical tropopause region, *J. Geophys. Res.*, *111*, D04104, doi:10.1029/2005JD006301.

Birner, T. (2010), Residual circulation and tropopause structure, *J. Atmos. Sci.*, *67*, 2582–2600.

Birner, T., A. Dörnbrack, and U. Schumann (2002), How sharp is the tropopause at midlatitudes?, *Geophys. Res. Lett.*, *29*(14), 1700, doi:10.1029/2002GL015142.

Bjerknes, J., and E. Palmen (1937), *Investigation of Selected European Cyclones by Means of Serial Wscents*, vol. 12, 62 pp., Am. Meteorol. Soc., Boston.

Bush, A. B. G., and W. R. Peltier (1994), Tropopause folds and synoptic-scale baroclinic wave life cycles, *J. Atmos. Sci.*, *51*, 1581–1604.

Castanheira, J. M., J. A. Añel, C. A. F. Marques, J. C. Antuña, M. L. R. Liberato, L. de la Torre, and L. Gimeno (2010), Increase of upper troposphere/lower stratosphere wave baroclinicity during the second half of the 20th century, *Atmos. Chem. Phys.*, *9*, 9143–9153.

Hartmann, D. L. (2000), The key role of lower-level meridional shear in baroclinic wave life cycles, *J. Atmos. Sci.*, *57*, 389–401.

Holton, J. R., P. H. Haynes, M. E. McIntyre, A. R. Douglass, R. B. Rood, and L. Pfister (1995), Stratosphere-troposphere exchange, *Rev. Geophys.*, *33*, 403–439.

Kochanski, A. (1955), Cross sections of the mean zonal flow and temperature along 80, *J. Meteorol.*, *12*, 95–106.

Kunz, A., P. Konopka, R. Müller, L. L. Pan, C. Schiller, and F. Rohrer (2009), High static stability in the mixing layer above the extratropical tropopause, *J. Geophys. Res.*, *114*, D16305, doi:10.1029/2009JD011840.

Miyazaki, K., S. Watanabe, Y. Kawatani, Y. Tomikawa, M. Takahashi, and K. Sato (2010), Transport and mixing in the extratropical tropopause region in a high-vertical-resolution GCM. Part I: Potential vorticity and heat budget analysis, *J. Atmos. Sci.*, *67*, 1293–1314.

Pan, L. L., W. J. Randel, J. C. Gille, W. D. Hall, B. Nardi, S. Massie, V. Yudin, R. Khosravi, P. Konopka, and D. Tarasick (2009), Tropospheric intrusions associated with the secondary tropopause, *J. Geophys. Res.*, *114*, D10302, doi:10.1029/2008JD011374.

Plougonven, R., and C. Snyder (2007), Inertia-gravity waves spontaneously generated by jets and fronts. Part I: Different baroclinic life cycles, *J. Atmos. Sci.*, *64*, 2502–2520.

Polvani, L. M., and J. G. Esler (2007), Transport and mixing of chemical air masses in idealized baroclinic life cycles, *J. Geophys. Res.*, *112*, D23102, doi:10.1029/2007JD008555.

Randel, W. J., and F. Wu (2010), The polar summer tropopause inversion layer, *J. Atmos. Sci.*, *67*, 2572–2581.

Randel, W. J., D. J. Seidel, and L. L. Pan (2007a), Observational characteristics of double tropopauses, *J. Geophys. Res.*, *112*, D07309, doi:10.1029/2006JD007904.

Randel, W. J., F. Wu, and P. Forster (2007b), The extratropical tropopause inversion layer: Global observations with GPS data, and a radiative forcing mechanism, *J. Atmos. Sci.*, *64*, 4489–4496.

Rotunno, R., C. Snyder, and W. C. Skamarock (1994), An analysis of frontogenesis in numerical simulations of baroclinic waves, *J. Atmos. Sci.*, *51*, 3373–3398.

Schmidt, T., G. Beyerle, S. Heise, J. Wickert, and M. Rothacher (2006), A climatology of multiple tropopauses derived from GPS radio occultations with CHAMP and SAC-C, *Geophys. Res. Lett.*, *33*, L04808, doi:10.1029/2005GL024600.

Shepherd, T. G. (2002), Issues in stratosphere-troposphere coupling, *J. Meteorol. Soc. Japan*, *80*, 769–792.

Simmons, A. J., and B. J. Hoskins (1980), Barotropic influences on the growth and decay of non-linear baroclinic waves, *J. Atmos. Sci.*, *37*(8), 1679–1684.

Skamarock, W. C., J. B. Klemp, J. Dudhia, D. O. Gill, D. M. Barker, M. G. Duda, X.-Y. Huang, W. Wang, and J. G. Powers (2008), A description of the Advanced Research WRF Version 3, *NCAR Tech. Note 468+STR*, Natl. Cent. for Atmos. Res., Boulder, Colo.

Snyder, C., W. C. Skamarock, and R. Rotunno (1991), A comparison of primitive-equation and semigeostrophic simulations of baroclinic waves, *J. Atmos. Sci.*, *48*, 2179–2194.

Son, S. W., and L. M. Polvani (2007), The dynamical formation of an extra-tropical tropopause inversion layer in a relatively simple general circulation model, *Geophys. Res. Lett.*, *34*, L17806, doi:10.1029/2007GL030564.

Stohl, A. P., et al. (2003), Stratosphere-troposphere exchange: A review, and what have we learned from STACCATO, *J. Geophys. Res.*, *108*(D12), 8516, doi:10.1029/2002JD002490.

Thorncroft, C. D., B. J. Hoskins, and M. E. McIntyre (1993), Two paradigms of baroclinic wave life-cycle behaviour, *Q. J. R. Meteorol. Soc.*, *119*, 17–55.

Whitaker, J. S., and C. Snyder (1993), The effects of spherical geometry on the evolution of baroclinic waves, *J. Atmos. Sci.*, *50*, 597–612.

Wirth, V. (2003), Static stability in the extratropical tropopause region, *J. Atmos. Sci.*, *60*, 1395–1409.

Wirth, V. (2004), A dynamical mechanism for tropopause sharpening, *Meteorol. Z.*, *13*, 477–484.

World Meteorological Organization (1957), *Meteorology: A Three-Dimensional Science: Second Session of the Commission for Aerology*, *WMO Bulletin*, vol. IV, pp. 134–138, World Meteorol. Org., Geneva.

Zhang, F. (2004), Generation of mesoscale gravity waves in the upper-tropospheric jet-front systems, *J. Atmos. Sci.*, *61*, 440–457.

L. M. Polvani, Departments of Applied Physics and Applied Mathematics and Earth and Environmental Sciences, Columbia University, New York, NY 10027, USA.

S. Wang, Department of Applied Physics and Applied Mathematics, Columbia University, New York, NY 10027, USA. (sw2526@columbia.edu)